Faradaic Reactions' Mechanisms and Parameters in Charging of Oils

Abhilash Sankaran, Chris Staszel, Farzad Mashayek, Alexander L. Yarin*

Department of Mechanical and Industrial Engineering, University of Illinois at Chicago, Chicago, IL 60607, USA

KEYWORDS: Leaky dielectric, Faradaic reactions, Electrohydrodynamics, Oil

ABSTRACT

Leaky dielectric liquids, e.g. oils, constitute a class of conductors capable of being electrified to possess a net charge. Faradaic reactions have been recently demonstrated to be responsible for the electrification of such liquids as canola oil in electrostatic atomizers. Here we explain the fundamental chemical kinetics of the mechanisms responsible for charging of these oils at metallic electrodes and measure their parameters. Three main mechanisms of the electrode faradaic reactions of oil are recognized. (i) Cathodic reduction of protons resulting from fatty acid dissociation accompanied by anodic reactions with formation of metallo-organic deposits (metal salts of fatty acids). (ii) Redox reactions with the participation of dissociated water

* Corresponding author, email:ayarin@uic.edu

molecules (the impurities) absorbed from the surrounding humidity; (iii) redox reactions on a sharp pin electrode (either being a cathode or an anode) at higher voltages (with the magnitude above about 4 kV) leading to the Coulombic repulsion of charged oil from this electrode and the emergence of a toroidal vortex-like circulation in the oil bath. The electrochemical findings are corroborated by the results obtained by means of the Infrared spectroscopy and Raman spectroscopy of the electrode deposits, and the introduction of a novel method of measurement of the electric conductivity of oils used to establish the kinetic constants of the Frumkin-Butler-Volmer kinetics in the form of the Tafel plot.

INTRODUCTION

The concept of the leaky dielectric model was introduced in the mid-1960s to explain the electrically-driven behavior of such seemingly insulating liquids as, for example, transformer oils [1-3]. The leaky dielectrics, which are essentially poor ionic conductors, possess an electric conductivity and are capable of polarization and/or electrification, revealing a net bulk charge in the polarized near-wall layers due to the intrinsic electro-kinetics mechanisms [4-5]. Conductivity of such liquids has been measured, albeit being very small [6]. The existence of ions in leaky dielectric liquids is attributed to dissociated impurities [7], to self-dissociation under strong electric fields, or to direct charge injection [8], and essentially its origin is still debated.

Electrochemical reactions were shown to be a contributing factor responsible for electrification of oil in electrostatic atomizers [9]. This implies that such ‘dielectric fluids’ as oils are essentially weak electrolytes, i.e. leaky dielectrics [3-4] with a possibility of faradaic

reactions responsible for charge transfer at the electrode surfaces. Since oils were not in focus of electrochemistry for a long time, the nature and origin of charge carriers in oils are still a mystery. In hydrocarbon oils, they are either attributed to impurities present or to spontaneous dissociation of oil molecules [10-11]. Water is considered one of the major impurities and is shown to have significant effect on conductivity of hydrocarbon liquids [12,13]. Unsaturated organic liquids with polarizable structures (like the carbonyl group) can absorb significant quantities of water [13]. Such liquids, including vegetable oils, are typically thought to contain several hundreds of ppm of water and can dissolve more than 1000 ppm of water at saturated conditions [13,14]. Vegetable oils are in focus in the framework of the electrostatic atomization, in particular, in relation to the food-processing industry and formation of carcinogenic compounds. Triglycerides are the main components of vegetable oils. Triglycerides possess three fatty acids on a glycerol backbone. The general structure of a triglyceride is shown in Figure 1. Overall, the R groups can be saturated or unsaturated long hydrocarbon chains. For example, the fatty acid constituents of canola oil [15] used in the present experiments are listed in Table 1.

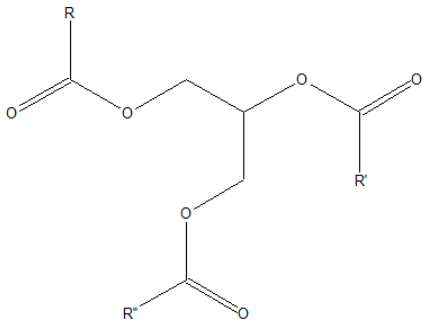

Figure 1. General structure of triglycerides with different possible combinations of long-chain fatty acids.

Table 1. Fatty acids in canola oil [15].

Acid	Formula	wt.%	Number of C atoms
Oleic	$CH_3(CH_2)_7CH=CH(CH_2)_7COOH$	60	18
Linoleic	$CH_3(CH_2)_4CH=CHCH_2CH=CH(CH_2)_7COOH$	20	18
Linolenic	$CH_3CH_2CH=CHCH_2CH=CHCH_2CH=CH(CH_2)_7COOH$	10	18
Stearic	$CH_3(CH_2)_{16}COOH$	2	18
Palmitic	$CH_3(CH_2)_{14}COOH$	4	16

In addition to triglycerides, oils include micro-constituents. Some of them, such as tocopherols (i.e. vitamin E, sometimes added on purpose), exist naturally. Some others, such as peroxides (compounds with an oxygen-oxygen single bond), free fatty acids (FFA), etc., could result from degradation during processing or storage. It should be emphasized that tocopherols are antioxidants which scavenge free radicals, while autoxidation or hydrolysis of vegetable oil result in free fatty acids (FFA) among other products. Additionally, one may refer to the CODEX standard for the whole range of additives, micro-constituents and their accepted levels in refined vegetable oil [16].

Production of vegetable oils involves different degrees of heating used to increase the yield. In heated or fried (e.g. for cooking) oils, the above-mentioned content of micro-constituents can change [15,17-19]. The content of tocopherol (vitamin E) in palm oil decreases at elevated temperatures [17]. For example, heating palm oil at 255 °C for 15 min led to a decrease of tocopherol concentration from 79.9 mg/L to 64.1 mg/L [18]. In the case of soybean

oil, the peroxide content was reported to marginally increase in time (on the scale of hours) during frying [18].

The literature dealing with oil pyrolysis listed numerous products resulting from oil cracking. One of the most typical first reactions during oil pyrolysis is given in Figure 2. The radicals RCHCO formed in such reactions further decompose into smaller compounds [15]. However, one of the common consequences of heating/frying of oil is an increase in the free fatty acid content in the oil. A study on pure tricaprin (representing saturated essential oil), which was heated at 190 °C for 3 h in a slow stream of dry air revealed formation of 2.5 % FFA [19]. Free fatty acids listed in Table 1 are weak carboxylic acids. FFA may be also considered as a weak electrolyte, albeit too weak when compared to the traditional carboxylic acid electrolytes, such as acetic and formic acids.

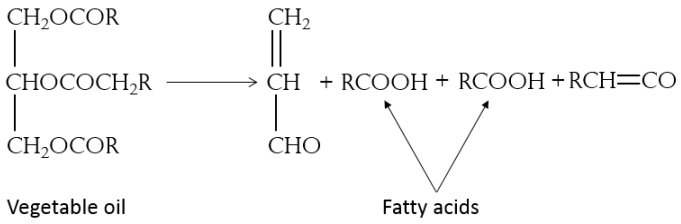

Figure 2. Decomposition of vegetable oil at pyrolysis temperatures producing fatty acids [15].

In the electrostatic atomizers [8], electrodes are perfect conductors (metals attached to a battery). Such electrodes sustain electric current, have zero tangential electric field (being iso-potential as conductors) and also sustain Faradaic reactions [9,20]. Essentially the faradaic reactions at the electrodes operating in the kinetics-limited regime (rather than in the diffusion-limited regime) are responsible for liquid electrification. Using certain similarity with gas

ionization, the slow faradaic reactions are called 'glowing' reactions, as it is done, for example, in relation to the corrosion reactions [21], or in general in the electrochemistry [22]. The kinetics of faradaic reactions follow the Butler-Volmer law [22,23], or the Frumkin-Butler-Volmer law [22,23] (with the presence of the polarized layer being accounted for).

The following sections describe the kinetics mechanisms of faradaic reactions in oils in detail: first, the reactions associated with fatty acids and resulting in formation of metallo-organic deposits (metal salts of fatty acids) on the anode; second, the reactions associated with the impurities (the water molecules); and third, the reactions associated with charging of neutral oil molecules at high voltages. The electrochemical findings are interpreted in the framework of the Frumkin-Butler-Volmer law and conclusions are drawn at the end.

FARADAIC REACTIONS IN OILS INVOLVING FATTY ACIDS

The electrode reactions can be attributed in the first approximation solely to the free fatty acids present in oil. The free fatty acids may dissociate according to the following reaction

$$RCOOH \rightarrow RCOO^{-} + H^{+} \quad (1)$$

where RCOOH stands for a general fatty acid.

Then, the following two overall faradaic reactions can occur at the electrodes. Namely, the overall cathodic reduction of hydrogen

$$2H^{+} + 2e^{-} \rightarrow H_2 \quad (2)$$

and the anodic oxidation reaction

$$RCOO^{-} + M \rightarrow RCOO^{-}M^{+} + e^{-} \quad (3)$$

where M stands for an anode metal involved in the reaction. Note that the anodic reaction (3) is quite similar to the formation of soap molecules which are sodium or potassium salts of fatty acids.

The question is whether the anodic reaction (3) is possible with such typical atomizer electrode materials as the transition metals like iron, nickel, etc. (involved in stainless steel) or zinc and copper (like in brass), which possess valences higher than one, and the R groups, which are bulky and thus limiting possible spatial configurations. It should be emphasized that the above-mentioned transition metals are known to form metallo-organic complexes with organic molecules and ions, which are called chelated compounds or coordination complexes. In particular, the carboxylic acids (e.g. naphthenic and capric acids), can be used as metal extractants [24]. The structures of these acids are depicted in Figure 3. Capric acids, which possess long chain carboxylic acids, are fatty acids found in coconut oil. Accordingly, it is plausible to imply that the anodic reactions (3) are possible in oils. Some of the coordination complexes resulting from the anodic reactions (3) with naphthenic and capric acid are listed Table 2 [24].

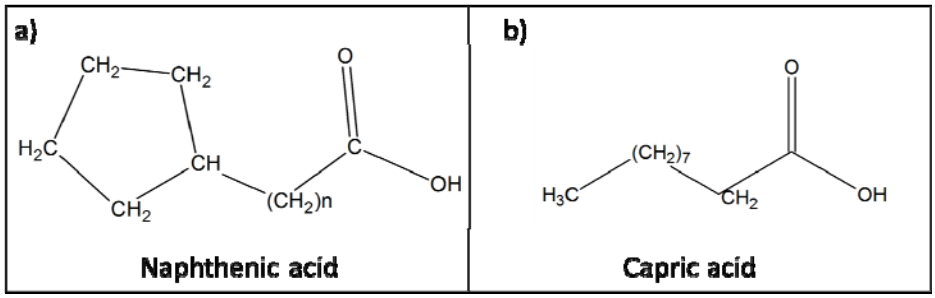

Figure 3. Structure of (a) naphthenic and (b) capric acid.

Table 2. Coordination complexes formed by different metals in reaction (3) [24], with RCOOH being the corresponding acid and RCOO being the resultant anion.

Naphthenic acid	**Capric acid**
$Ni_2(RCOO)_4 \cdot 4RCOOH$	$(Ni(RCOO)_2 \cdot 2RCOOH)_2$
$Co_2(RCOO)_4 \cdot 4RCOOH$	$(Cu(RCOO)_2 \cdot RCOOH)_2$
$Fe(RCOO)_3 \cdot RCOOH$	$(Co(RCOO)_2 \cdot 2RCOOH)_2$
	$(Fe(RCOO)_3)_3$

A number of coordination complexes formed by fatty acids and heavy metals in reaction (3) in different oils are of particular interest to the oil paint industry [25]. In such cases the complexes are formed due to the reaction of the added pigments containing metals and the fatty acids present in vegetable oil. Zinc carboxylates, such as zinc stearate and zinc palmitate, are commonly reported in relation to oil painting [25].

Summarizing the previous findings in the literature related to the cathodic and anodic reactions of oils, the following reactions can be formulated for an oil containing capric acid in the case of a copper anode. The overall cathodic reaction associated with Eq. (2):

$$\left[2H^+ + 2e^- \rightarrow H_2\right] \times 2 \tag{4}$$

and the anodic reaction associated with Eq. (3):

$$4RCOO^- + 2Cu + 2RCOOH \rightarrow \left(Cu^{2+}\left(RCOO^-\right)_2 \cdot RCOOH\right)_2 + 4e^- \tag{5}$$

Here, a total of four electrons are involved in the complete reaction.

As mentioned above, vegetable oils can contain vitamins, while the electrostatic atomizer electrodes can contain some other transition metals, rather than copper. The other transition metals can also be expected to form coordination complexes with different fatty acids and tocopherol (vitamin E) present in vegetable oils. The electrochemical behavior of the α, β, γ and δ isomers of tocopherol has been reported [26]. The neutral, reduced and oxidized forms of α-tocopherol are depicted in Figure 4. Accordingly, the cation and anion forms of α-tocopherol can participate in the reduction and oxidation cathodic and anodic faradaic reactions of types (2) and (3) and be responsible for oil charging and the electric current transport in oils. Generally, antioxidants are thought to chelate transition metals [27]. In particular, iron chelating ability is usually utilized to compare different antioxidant activities [28].

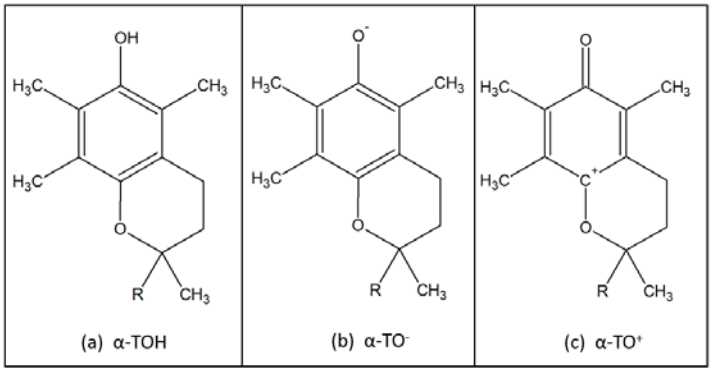

Figure 4. Structure of (a) neutral α-tocopherol, (b) tocopherol anion and (c) tocopherol cation [26].

One of the common elements containing a lone pair of electrons present in constituents of oil is oxygen [16]. Moreover, there are no other potential species that can act as ligands. This

results in the formation of coordination compounds of transition metals on anode with the oxygen-containing moieties acting as ligands.

EXPERIMENTAL

Experimental setup for observations of metallo-organic deposits on anode resulting from fatty acids and/or tocopherol. Figure 5 depicts the sketch of the experimental setup, which was used to form sufficient amounts of electrode deposits due to faradaic reactions.

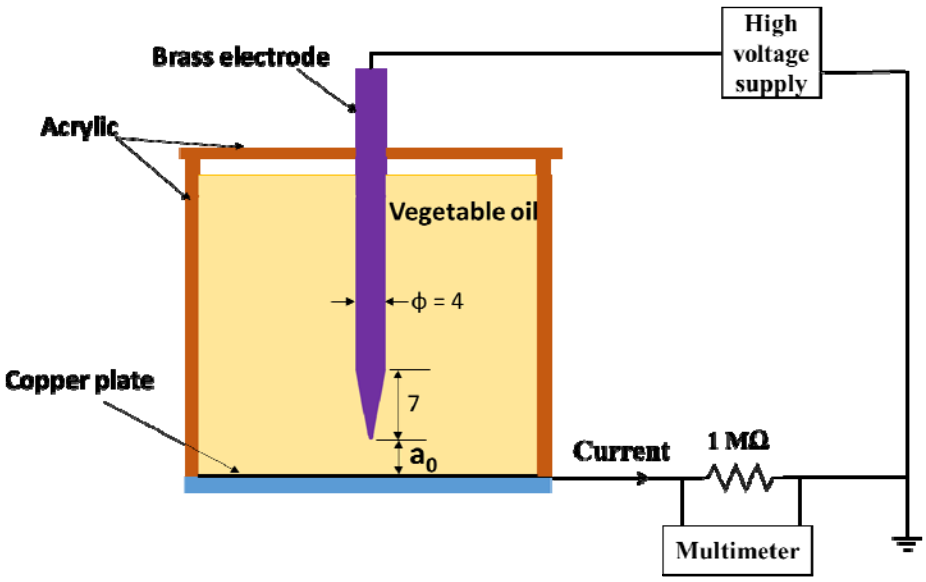

Figure 5. Schematic of the experimental setup used to form the electrode deposits. Dimensions are in mm.

The setup consisted of a brass (alloy 360) pin cathode submerged in a food-grade canola oil, with a copper plate (99.99%) being a counter-electrode. The bath of cross-section 102 mm × 102 mm was filled with ~ 500 mL of oil. The inter-electrode distance, a_0, was set at 1.8 mm using a spring-loaded micrometer with a resolution of 0.001 mm. The pin electrode was connected to a custom-built negative high voltage (0-20 kV) DC supply. The counter-electrode copper plate was connected to ground through a 1 MΩ external resistor. A multimeter (HP model

3478A) was connected in parallel with the 1 MΩ resistor to measure the voltage drop. The total electric current through oil was then found using Ohm's law applied to the resistor. The applied voltage was kept well below the spark regime, which if happened, would no longer be in the electrochemical range and is not the operating condition desired in typical applications. To verify the absence of sparking, an additional experiment with ramping of the applied voltage was conducted. It revealed a spark at -14.5 kV. Therefore, in the present experiments the applied voltage was kept well below this sparking regime. Note also, that since the current was continuously monitored, a spark would interrupt the measurements, which did not occur confirming that there was no spark in the present experiments.

Formatted: Highlight

It should be emphasized that the passage of the electric current through the inter-electrode gap implies joule heating there. At high values of the applied voltage it might become significant to trigger an 'ignition'-like phenomenon (sparking) arising due to the fact that the electrical conductivity is an exponentially growing function of temperature. Such critical phenomena deserve a separate investigation and will be studied in future.

Formatted: Highlight

The experiments using the setup of Figure 5 were conducted for extended periods of time up to 20 h, long enough for perceivable amount of surface reaction products being accumulated on the electrode, and indeed, a sufficient amount of reaction products was observed on the copper counter-electrode plate. According to Faraday's first law, the mass of products accumulated on an electrode is proportional to the total electric charge passed. Typical currents of the order of 0.1-1 μA were measured when the voltages up to -12 kV were applied to the cathode pin. As an estimate, the molecular mass of oil is about 100 g/mol, which would result in the total products mass deposited for 24 h due to faradaic surface reactions of the order of 0.01-0.1 mg. Such low amounts of products indicate the difficulty in direct application of some of the

characterization techniques, e.g. the X-Ray Diffraction or quantification using the Atomic Absorption Spectra. Even with such a miniscule expected deposit formation, some intriguing features were found on the counter-electrode after these long experiments, as discussed below. FTIR spectra of the deposit samples were recorded by Bruker ALPHA II Platinum ATR spectrometer in the 400-4000 cm^{-1} range. Raman spectra of the deposit were obtained by using green 532 nm laser and the instrument Renishaw inVia Reflex Raman.

Measurement of the electric current, conductivity and kinetic constants of faradaic reactions of oil. A modified version of the setup depicted in Figure 5 allowed for a direct measurement of the electrical conductivity of oil used to deduce the kinetic constants of the Frumkin-Butler-Volmer mechanism of faradaic reactions. This modified setup is shown in Figure 6a. In this setup, most of the pin electrode, except the area near the tip is covered by an insulation silicone layer. The stainless steel (alloy 303) pin electrode was submerged in an oil bath with a grounded stainless steel plate (alloy 303). In addition, stainless steel counter-electrode was chosen as there were no visual pits formed (in distinction from a copper counter-electrode, as discussed later). The experiments were performed in a small room where the humidity was maintained at RH 33±3 % with the help of dehumidifier (GE ADEL70LR).

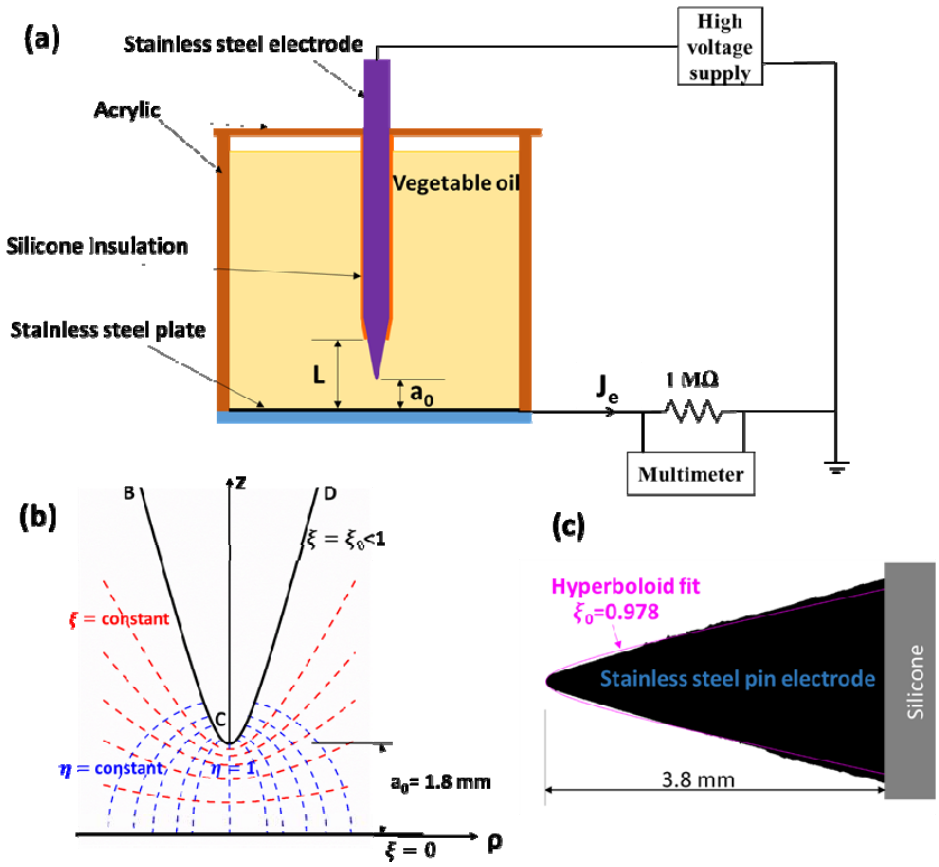

Figure 6. (a) Experimental setup with the tip electrode partially covered with silicone insulation. This setup was used to measure the electrical conductivity of oil. (b) Sketch of a hyperboloidal pin electrode with prolate spheroidal coordinate system ξ and η. (c) Photograph of the stainless steel electrode used in the experiments and its fit by the hyperboloid of revolution shown by pink line. The corresponding values of a_0 and ξ_0 are a_0 = 1.8 mm and ξ_0= 0.978. The entire setup was placed inside a Faraday cage to keep the electrical noise to minimum.

Fundamentals of the novel method of measurements of the electric conductivity of oil using the setup of Figure 6. The pin electrode can be closely approximated by a hyperboloid of revolution (BCD in Figure 6b) located near the grounded counter-electrode [29-31]. The tip of the hyperboloid BCD (the pin electrode, Figure 6c) sustained at voltage $\Phi=V_0$ (with V_0 being either positive or negative) is located at a distance a_0 from the grounded counter-electrode (the equipotential surface $z = 0$). To find the potential distribution in the inter-potential domain, it is convenient to use the prolate spheroidal coordinates $0 \le \xi \le \xi_0 < 1$ and $1 \le \eta \le \infty$. The surface of the hyperboloid BCD (the pin electrode of Figure 6c)

$$\frac{z^2}{a_0^2} - \frac{\rho^2 \xi_0^2}{a_0^2\left(1-\xi_0^2\right)} = 0 \qquad (6)$$

corresponds to $\xi = \xi_0$ (see Figures 6b and 6c). The cylindrical coordinates ρ and z are shown in Figure 6b. The coordinate iso-lines are also shown in Figure 6b, with the lines $\eta =$ constant corresponding to ellipsoids, and the lines $\xi =$ constant corresponding to hyperboloids.

Since oil is electroneutral in the bulk, and even in the polarized layers near the electrodes the ion effect on the potential is negligible because the net charge there is small due to minute ion concentrations (at least up to $|V_0|$ =4 kV), the field of the electric potential Φ is found as a solution of the Laplace equation. In the prolate spheroidal coordinates it reads [29-31]

$$\Phi = V_0 \frac{\ln\left[\left(1+\xi\right)/\left(1-\xi\right)\right]}{\ln\left[\left(1+\xi_0\right)/\left(1-\xi_0\right)\right]} \qquad (7)$$

with the detailed description of the solution method available elsewhere [30]. In the experiments, the pin electrode was a cathode sustained at $\Phi=V_0$, with V_0 in the -1 to -4 kV range.

Formatted: Highlight

Accordingly, the electric current density $\mathbf{j}_e$ is found from Ohm's law, $\mathbf{j}_e = -\sigma\nabla\Phi$, with σ being the electrical conductivity. The vector of the electric current density at metal electrodes is normal to their surfaces, since they are conductors. In particular, at the surface of the pin electrode according to Eqs. (6) and (7) the magnitude of the electric current density at the pin is found as

$$j_e = \frac{2\sigma(-V_0)}{\ln\left[(1+\xi_0)/(1-\xi_0)\right]\sqrt{1-\xi_0^2}\sqrt{z^2/\xi_0^2 - a_0^2}} \tag{8}$$

Using Eq. (8), the magnitude of the total electric current, J_e, in the system is found as

$$J_e = \int_{a_0}^{L} j_e 2\pi\rho\sqrt{1+\left(\frac{\partial\rho}{\partial z}\right)^2}\,dz = \frac{4\pi\sigma(-V_0)}{\xi_0\ln\left[(1+\xi_0)/(1-\xi_0)\right]}(L-a_0) \tag{9}$$

where L corresponds to the distance from the counter-electrode to the beginning of the insulated part of the pin electrode (see Figure 6c, where $z=a_0$=1.8 mm corresponds to the electrode tip and z=L=1.8 mm + 3.~~28~~5 mm = 5.~~05~~6 mm corresponds to the beginning of the silicone insulation layer). Note also that the area of the hyperboloidal pin electrode (Figure 6) is found as

$$A = \frac{\pi\sqrt{1-\xi_0^2}}{\xi_0^2}\left\{L\sqrt{L^2 - a_0^2\xi_0^2} - a_0^2\sqrt{1-\xi_0^2} - a_0^2\xi_0^2\ln\left[\frac{L+\sqrt{L^2 - a_0^2\xi_0^2}}{a_0 + a_0\sqrt{1-\xi_0^2}}\right]\right\} \tag{10}$$

Using Eq. (9), the electrical conductivity of oil can be found by measuring the total electric current, J_e, in the system at a fixed applied voltage (V_0). For such measurements, the stainless steel pin electrode was immersed in the canola oil bath (cf. Figure 6a), with the inter-electrode gap a_0 being 1.8 mm. This gap was fixed using a spring-loaded micrometer with a resolution of 0.001 mm. The pin electrode was connected to a custom-built negative high voltage (0-20 kV) DC supply. As depicted in Figure 6c, the pin electrode was covered by the insulating silicone layer to maintain the conducting tip length of 3.~~82~~5 mm, and hence L = 5.~~60~~5 mm (cf. Figure

Formatted: Highlight
Formatted: Highlight
Formatted: Highlight
Formatted: Highlight

6a). As in the setup of Figure 5, in the setup of Figure 6 the counter-electrode stainless steel plate was connected to ground through a 1 MΩ external resistor. A multimeter (HP model 3478A) was connected in parallel with the 1 MΩ resistor to measure the voltage drop. The total electric current through the oil, J_e, was then found using Ohm's law applied to the resistor.

RESULTS AND DISCUSSION

Anodic reactions and deposits. The electrochemical setup shown in Figure 5 was operated for 19 h at the cathode voltage of -12 kV with a measured average current around -0.45 μA. Due to such a long experimental time, a 'mound' of faradaic reaction products was formed on the copper counter-electrode plate. Upon completing the 19 h-long experiment, the setup was disassembled and the copper counter-electrode removed from the oil bath. Then, images of this mound were photographed at various angles using a DSLR camera with a 180 mm lens. These images are shown in Figure 7.

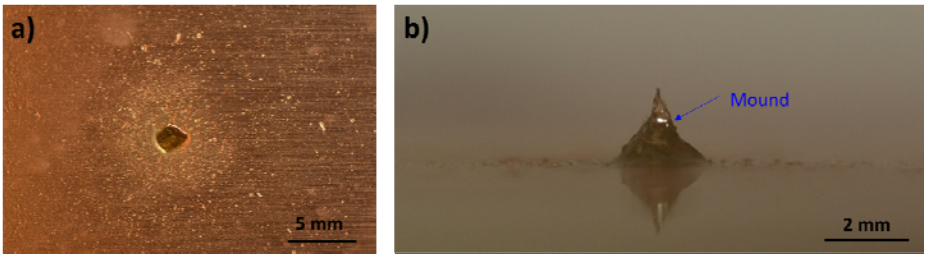

Figure 7. (a) Top view of the mound formed by the faradaic reaction products on the copper counter-electrode, and (b) an enlarged side view of the mound.

Figure 7b shows that the counter-electrode accumulated the mound of nearly the same height as the inter-electrode gap (1.8 mm). An estimate of the mound mass assuming it as a cone (with the base diameter of about 2.5 mm) revealed the mass of about 3 mg (using the oil density of 0.92 g/cm^3). From Faraday's first law, for the measured electric current discussed above, the expected deposited mass would be about 0.03 mg (assuming the characteristic molecular weight of 100 Da), which is 2 orders of magnitude smaller than to the estimated mound mass. ~~An estimate of the mound mass assuming it as a cone revealed the mass of ~1 g, which is 4 to 5 orders of magnitude higher than that expected from Faraday's first law.~~ This implies that most probably the mound stems from chemical changes of oil in strong electric field in addition to the products of faradaic reactions (also present in much smaller quantities). Accordingly, the idea that the mound is comprised of the products of the electrode faradaic reactions, in addition to the other chemical compounds which stem from the oil, seems plausible. Regarding the latter, note that the free fatty acid content can be increased upon treatment of vegetable oil with strong electric fields [32]. Infrared (IR) spectroscopy was employed to analyze the nature of the mound. However, no distinguishable difference in the spectrum of the mound from that of pure canola oil was found. It was assumed that the mound still contained a significant amount of oil or oil-like constituents in comparison to the expected faradaic reaction products. In particular, fatty acids and related compounds are known to form gelatinous consistency [33] in contact with vegetable oil.

This gelatinous consistency may be responsible for the fact that the shape of the mound did not change for many hours after the experiment was finished and it looked like a solid body as is seen in Figure 7. To verify that the mound was indeed gelatinous, rather than just a viscous liquid oil, additional images were taken approximately 20 h after the end of the experiment

Formatted: Highlight

(Figure 8b) and compared to the one taken immediately after the experiment (Figure 8a). No visible changes were found, which is impossible if such a structure would be a liquid subjected to the effects of gravity and surface tension. Accordingly, the mound was indeed a gelatinous structure.

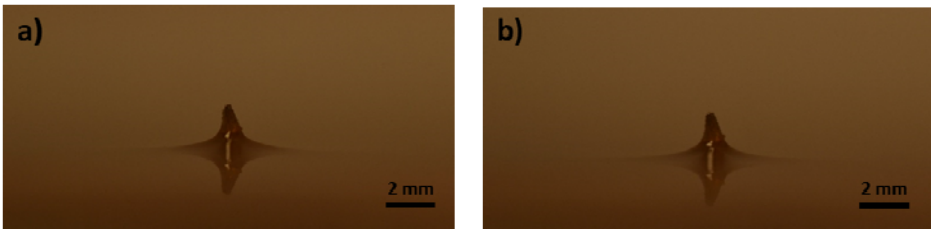

Figure 8. (a) Side view of the mound formed on the copper-counter electrode immediately after the end of the experiment, and (b) approximately 20 h after that.

An additional long-term experiment was conducted for 48 h at -12 kV with an average current of -0.45 μA. The surface was then dipped in heptane to remove most of the oil-like gelatinous substances but to leave the surface reaction products for analysis. As discussed in the section 'Faradaic reactions in oils involving fatty acids', metal salts are likely to be formed due to the electrode reactions with oil which are hardly soluble in heptane [34] in distinction from canola oil. The remaining deposit was scraped from the copper counter-electrode and transferred for characterization, which employed the Infrared (IR) Spectroscopy. The resulting spectrum of the deposit is shown in Figure 9 in comparison with the base oil spectrum.

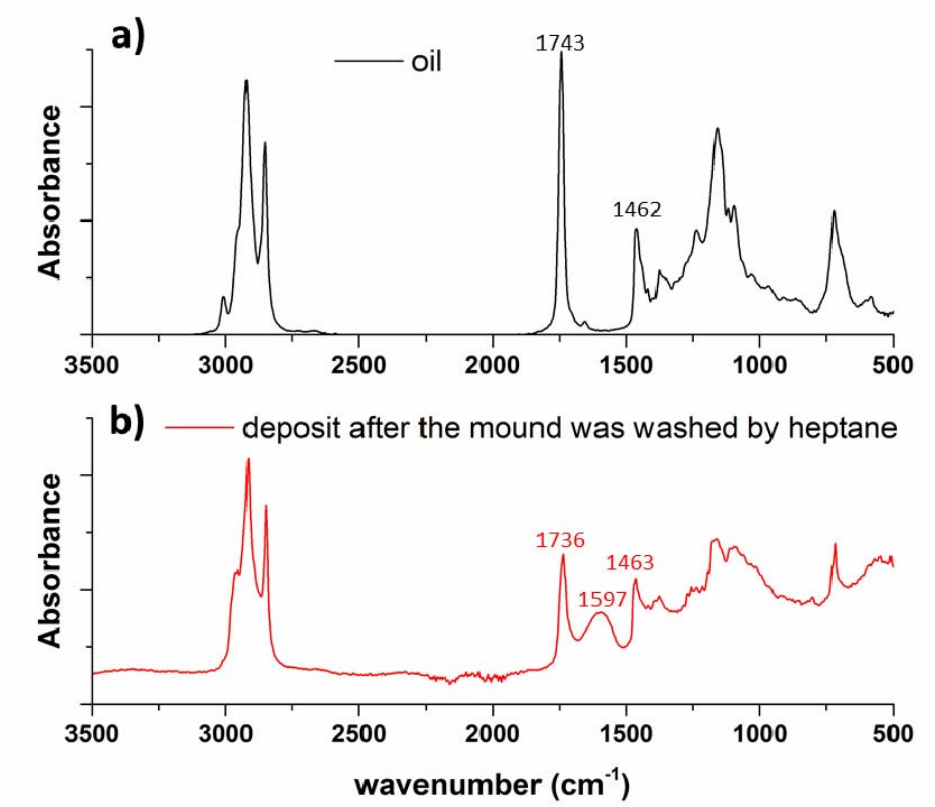

Figure 9. Infrared spectra of (a) the original canola oil and (b) the deposit left from the mound washed with heptane and scraped from the copper counter-electrode.

Figure 9 shows that the IR spectrum of the residual deposit revealed almost all the peaks characteristic of oil. However, one can clearly see an additional peak, though broad, at 1597 cm^{-1}. This additional peak corresponding to the deposit but not to pure canola oil in Figure 9 pertains to the metal carboxylates. The antisymmetric frequency of COO^- in the case of metal soaps is expected to be in the 1500 – 1650 cm^{-1} range [35,36]. Furthermore, it can be observed that the intensity of the peak near 1740 cm^{-1} associated with C=0 symmetric stretching has been reduced in the case of the deposit in comparison with canola oil (Figure 9). This is an indication of conversion of fatty acids into metal carboxylates [35]. A strong peak at ~ 1590 cm^{-1} was reported for the fatty acid salts of copper [35,36]. The broad peak at ~1597 cm^{-1} implies different ways a metal center can be bonded to the ligands, in addition to the possibility that some of the carboxylate groups may be replaced by other ligands, e.g. by dissolved water. It should be emphasized that no additional peaks are expected due to treatment with heptane, particularly, nothing related to CO bonds. Therefore, the present spectra confirm the kinetics of the anodic process detailed before, in particular, reactions similar to Eq. (5).

Additionally, a further cleaning of the deposit resulted in a discolored region underneath. An image of this discoloration on the copper counter-electrode is shown in Figure 10a, and the corresponding image of the discoloration obtained using the optical microscope Olympus BX51 is shown in Figure 10b in contrast to the image from the region far away (Figure 10c).

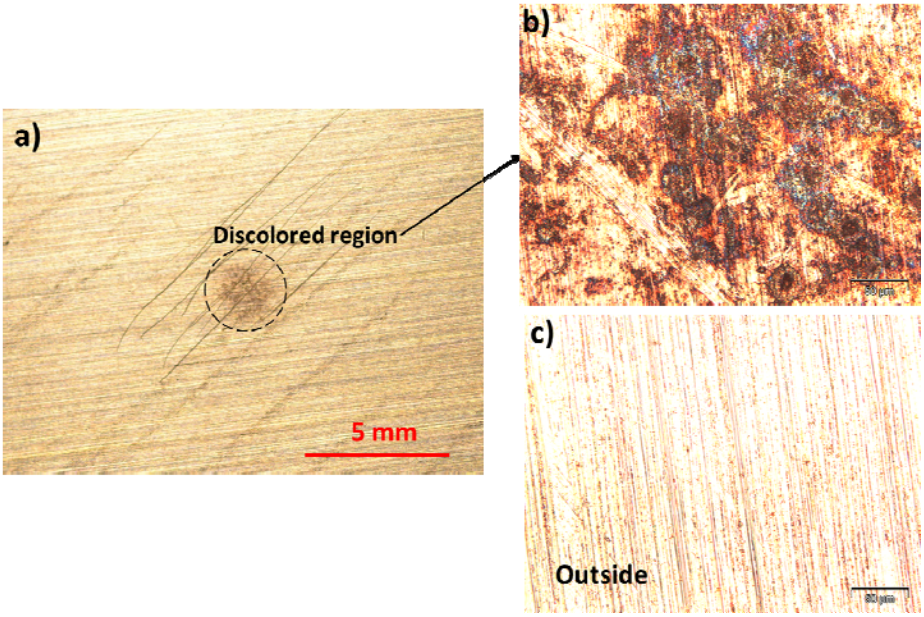

Figure 10. (a) The copper surface cleaned from the mound and deposit leaving a discolored region underneath. (b) The discolored region observed using optical microscope. (c) The region far away from the discoloration observed using optical microscope.

The optical microscope image of the discoloration (Figure 10b) reveals pits decorated by different colors including blue, pink and brown. These distinct colors are characteristics of different compounds of copper. In particular, the strong blue color can be directly related to azurite ($Cu_3(CO_3)_2(OH)_2$), which is a basic copper carbonate. In nature, one finds azurite with its relative - malachite ($Cu_2CO_3(OH)_2$) which is also a basic carbonate of copper - green in color. Although one does not recognize a characteristic green color in Figure 10b, its presence

cannot be ruled out. In addition, pink and brown colors clearly visible in Figure 10b can be attributed to copper (1) and copper (2) oxides, respectively.

Raman spectrum of the discolored region from another experimental trial was also obtained to complement the results discussed above. The results are shown in Figure 11. Note that these results were obtained at different spots within the discolored region.

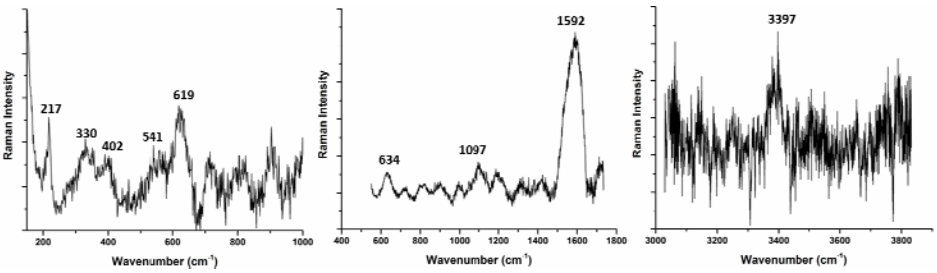

Figure 11. Raman spectrum of the discolored region.

The results of the Raman spectroscopy in Figure 11 exhibit the characteristic peaks of copper (1) oxide (218, 523 and 623 cm^{-1}) [37]. Additionally, some of the other peaks at smaller wavenumbers can also be attributed to copper carbonates (402, 1097 cm^{-1}) [38]. The peak at 1592 cm^{-1} can be attributed to the carbonate stretching vibration of azurite [38]. Furthermore, the peak at 3397 cm^{-1} is close to the hydroxyl stretching band related to azurite [38]. A more detailed comparison of the basic carbonates cannot be made from the observed spectra as the peaks are not distinct and many smaller peaks are found. The difficulty stems from the fact that these are surface features with different copper compounds in addition to copper itself as a background.

It is also worthwhile to compare the results obtained here to the corrosion study of copper in biodiesel [39] (which is a derivative from vegetable oil). In Ref. 39 it was assumed that the corrosion film consists of metal carboxylate, and indeed, the IR spectrum of the corrosion film revealed a peak near 1580 cm^{-1}. However, no interpretation was given to this peak in Ref. 39. Note that this peak is related to COO^- antisymmetric frequency attributed to metal carboxylates, which is observed in the IR spectrum of the deposit in our case. In addition, the X-ray powder diffraction (XRD) analysis of the exposed copper surface also revealed copper oxides and basic copper carbonates [39], in concert with the results presented here. Reference 39 also states that the basic carbonates form by a further decomposition of fatty acids in the presence of dissolved water and gases (carbon dioxide and oxygen). Namely, copper oxides being formed due to reaction with dissolved oxygen [39].

Similar experiments were also conducted with stainless steel as a counter-electrode. Visible deposits were observed in these experiments too, albeit with different characteristics. In the stainless steel case, the mound was comparatively flatter (in comparison to that of Figure 7), and there was no visible discolored region below the removed deposit. The mound was cleaned with heptane and the remnant deposit in the case of stainless steel is shown in Figure 12. In particular, Figure 12c reveals that a flaky chip of the brown material disappeared as a result of cleaning.

The IR spectrum of the deposit accumulated on the stainless steel counter-electrode revealed a shoulder at 1603 cm^{-1} (Figure 13b) non-existent in the oil spectrum (Figure 13a), which is probably related to the metal carboxylates, as discussed before.

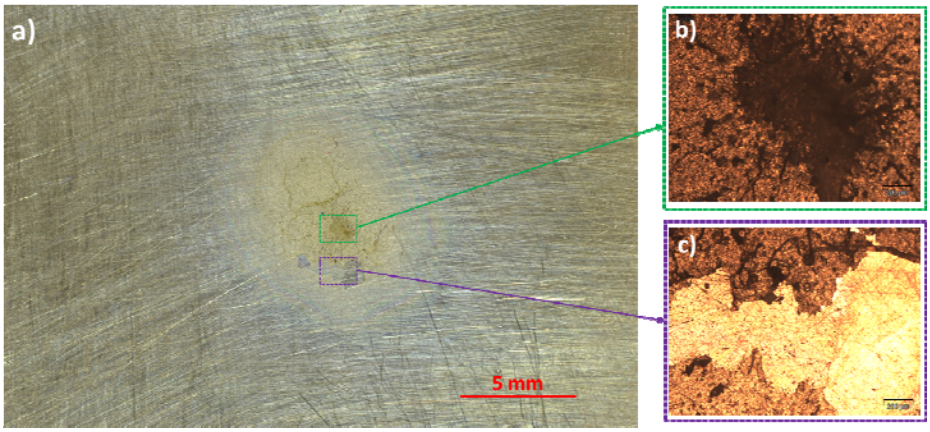

Figure 12. (a) The image of the stainless steel counter-electrode surface cleaned with heptane. (b) The optical microscope images of the deep brown deposit. (c) The area where a flaky chip of the brown material was removed by cleaning.

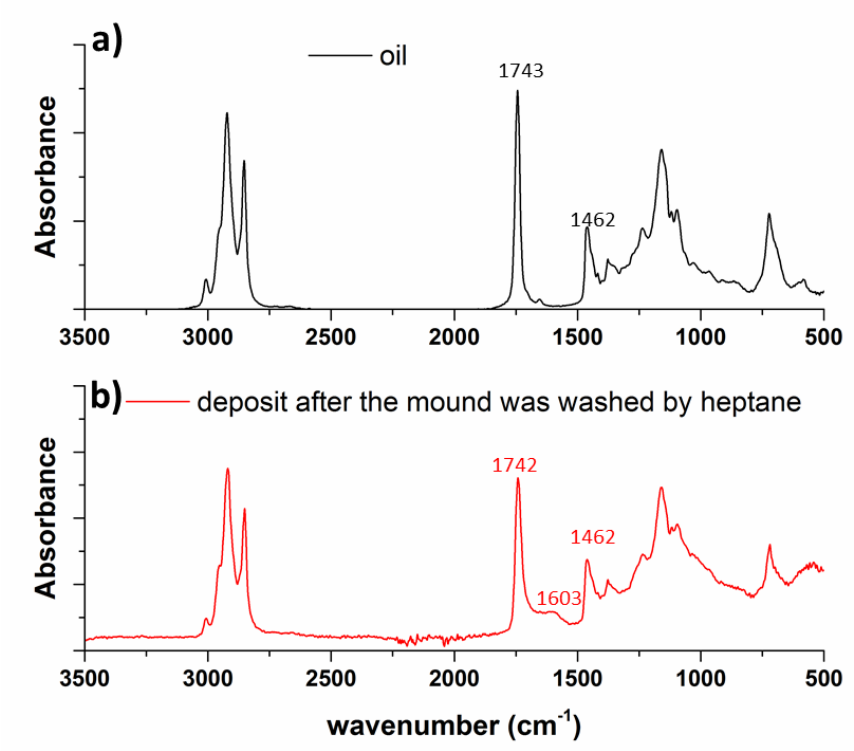

Figure 13. Infrared (IR) spectra of (a) the oil, and (b) of the deposit mound accumulated at the stainless steel counter-electrode and rinsed with heptane.

The effect of tocopherol in anodic reactions and oil charging could not be confirmed in the present case. Additional experiments were conducted, in which α-tocopherol was added into the canola oil. However, no differences in the deposits or measured electric currents were observed. This implies that tocopherol does not play significant role in charging of the canola oil.

Formatted: Highlight

Formatted: Indent: First line: 0.38"

Formatted: Font: Not Bold, Not Italic

Cathodic faradaic reactions. In the present work, no visible deposits on the cathode pin electrode was observed, which is interpreted as hydrogen reduction being taking place there. The origin of protons participating in this reaction is either in the fatty acids or tocopherol [cf. Eqs. (1) and (4)], or in the dissolved water, as discussed below. It should be emphasized that no bubbles was observed on the cathode in the present work, probably due to the low currents. However, such bubbles were observed in separate experiments with diesel fuel described in detail elsewhere (Ref. 40) and are shown in Figure 14. The bubbles are formed presumably from hydrogen resulting from reduced and recombined protons in the experiments conducted at a negative DC voltage supply to the blade cathode in Ref. 40.

Figure 14. Bubble observed on the sharp cathode blade in diesel fuel (Ref. 40).

Electrical current and conductivity. Two different regimes of the electrical current transfer were observed in the present experiments: (i) the quasi-ohmic regime at relatively low voltages, and (ii) the high-voltage regime with bulk liquid motion and significant convective component of the electric current [8,41,42]. This convective motion observed in our experiments is also discussed

in detail in one of the subsequent sections. Namely, at low magnitude of the applied potentials $|V_0| \leq 4$ kV, the measured current-voltage (I-V) characteristics revealed the quasi-ohmic regime, in which the electrical conductivity was measured. The experiments where the electrical conductivity was measured were conducted on a single batch of food-grade canola oil at room temperature (22 °C). The electric current was recorded every second for 5 min at each applied voltage, and time averaged for the last 4 min of the steady-state quasi-ohmic regime. This was done at $|V_0| = 1$, 2, 3, and 4 kV.

The self-consistency of the results was checked by changing the exposed length of the pin below the insulation layer (cf. Figure 6), effectively changing L. The current, as predicted by Eq. (9), is expected to increase proportional to the increase in L, with the other parameters being fixed within the quasi-ohmic regime. This is indeed, corroborated by the experimentally measured current as is seen in Figure 15, which confirms that convective current transport was negligibly small in the potential range up to $|V_0| = 4$ kV and resulted in a practically constant conductivity. Note that the hyperboloid fit does not properly fit the electrode as L increases, as shown in Figure 6, which introduces inaccuracies. However, the measured conductivity was still within the acceptable limits.

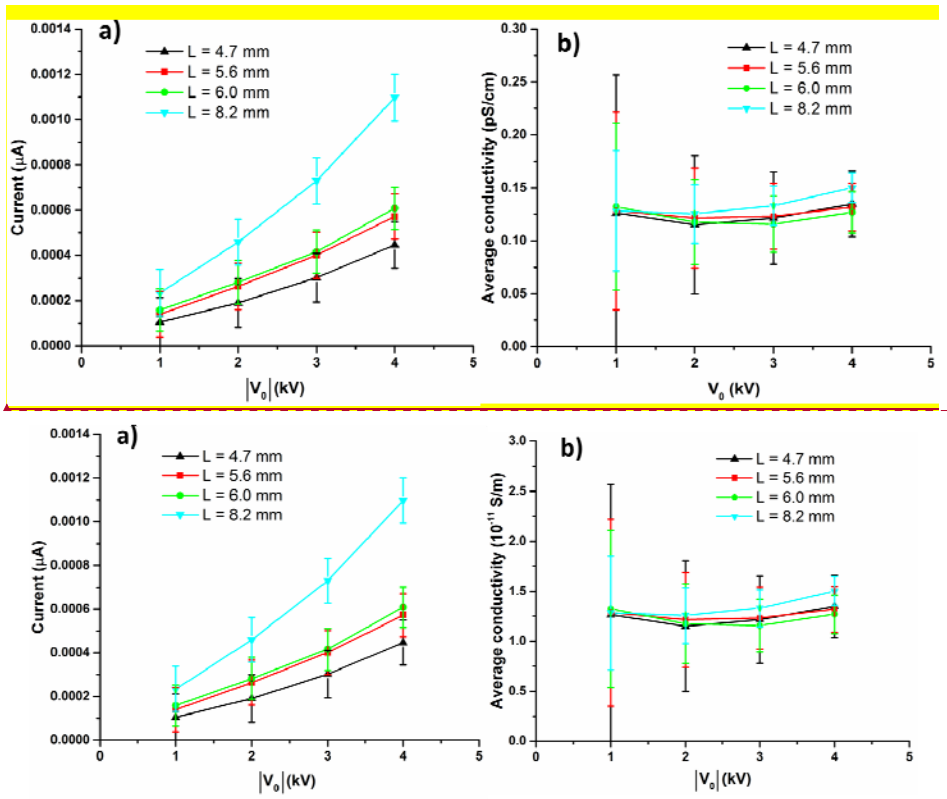

Figure 15. (a) Measured electric current at different lengths of the uninsulated pin. (b) The corresponding conductivity values deduced. In the experiments with canola oil the cathode pin was maintained at V_0= -1, -2, -3, and -4 kV.

Several additional experiments were conducted with the uninsulated pin length L being fixed at 5.6 mm. The time and ensemble averaged values of the measured electrical conductivity with the corresponding standard deviation values obtained from three trials are shown in Figure 16. The measured conductivity of canola oil is of the order of 0.1 pS/cm ~~10^{-11} S/m~~, which is in the range typically reported in literature for canola oil [43]. The increase of the standard deviation at

Formatted: Highlight

Formatted: Highlight

the voltage of about -1 kV stems from the limitations in small electric current measurements in the setup of Figure 5.

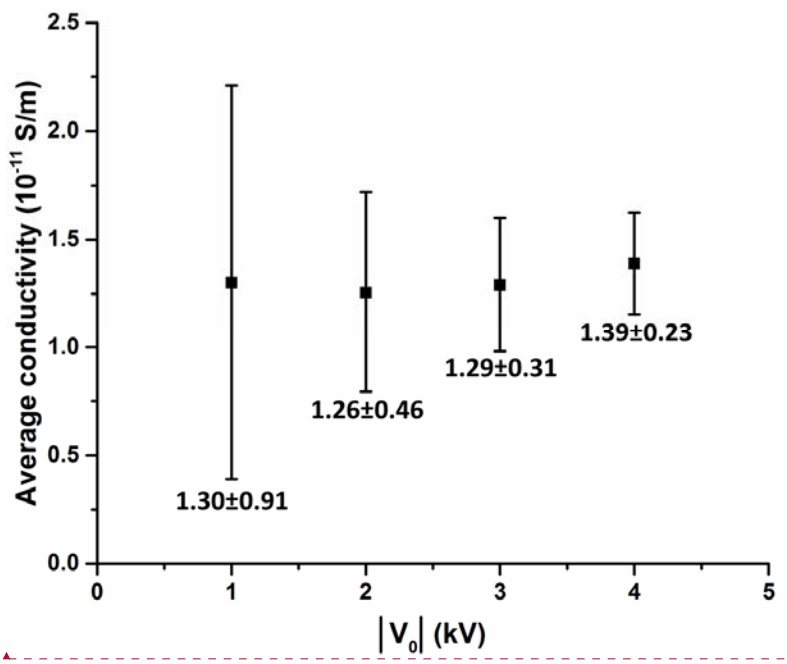

Formatted: Highlight

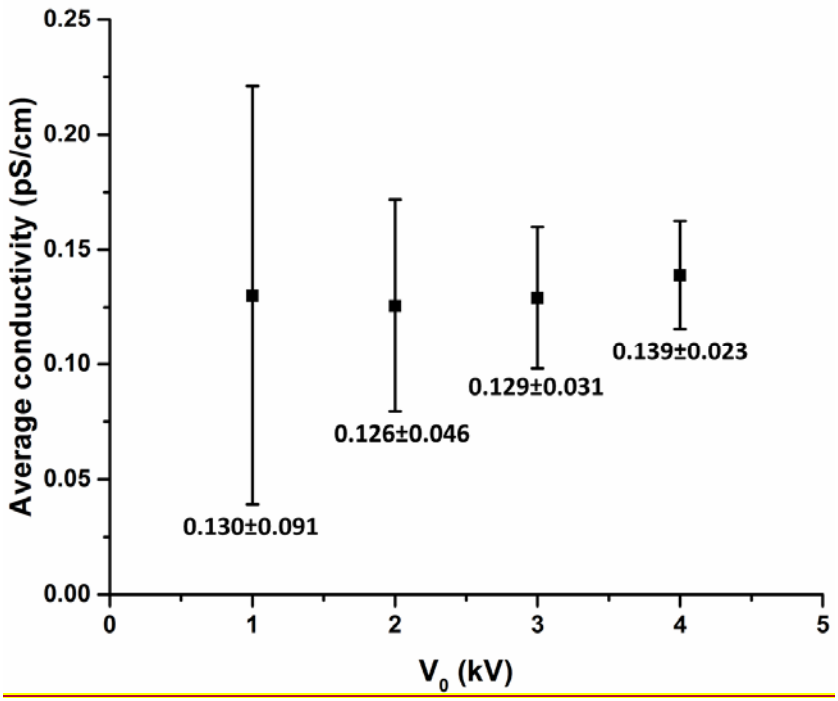

Figure 16. Electrical conductivity of canola oil with fixed L = 5.6 mm. In the experiments the cathode pin was maintained at V_0= -1, -2, -3, and -4 kV.

To further validate the novel method employed by the setup in Figure 6, comparison of the results with the data obtained using a commercial conductivity meter (D-2 inc. model JF-1A-HH-CM) was undertaken. The commercial conductivity meter measures conductivity in the range 0.0 – 2000.0 pS/cm. Accordingly, its accuracy is insufficient in the low-conductivity range expected for canola oil, since it is close to the lower limit of JF-1A-HH-CM. Therefore, comparison of the results from the setup of Figure 6 and JF-1A-HH-CM was done using a motor

oil (Castrol SAE10w-30) with a higher conductivity. The conductivity value for the Castrol SAE10w-30 oil found from 28 trials using the conductivity meter JF-1A-HH-CM was 216.7 ± 1.8 pS/cm at the average temperature 25 °C and the relative humidity (RH) of 50 %. The conductivity measured using the setup of Figure 6 in the -1.0 kV to -2.3 kV range (9 trials) was 216.9 ± 3.8 pS/cm at 22 °C and 38-41 % RH. It should be emphasized that at such low values of the applied voltage the uncertainty in the set voltage can be significant, since the lowest increment in the voltage supply is 0.1 kV.

Additionally, note that the JF-1A-HH-CM conductivity meter employs the AC-based measurements, whereas the present device (Figure 6) utilizes a DC source. Still, the conductivity values obtained by the two independent methods are close within the experimental uncertainties, which corroborates the novel approach introduced in the present work.

Effect of added oleic acid on the electric conductivity and faradaic reactions. Technical grade oleic acid (90%, Sigma Aldrich) was added to canola oil to assess a potential effect of added fatty acid. The measured electric current (using the setup of Figure 6) with oleic acid (10 g/L) added to canola oil is shown in Figure 17 in comparison to the base case of the same oil without added oleic acid. The results show that the addition of oleic acid did not alter the oil conductivity. This is probably related to the fact that the major component in the electric current, and thus the electrical conductivity, stems from dissolved water molecules, as discussed in the following subsection.

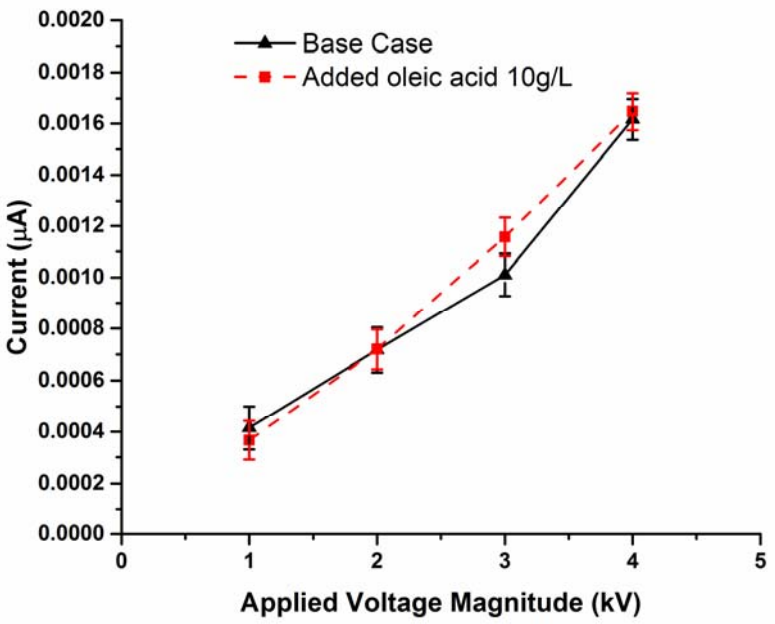

Figure 17. Comparison of the current-voltage dependences with and without (the base case) added oleic acid.

In addition, the long-term experiments using the setup of Figure 5 were conducted to compare qualitatively the deposits formed at the copper counter-electrode with and without added oleic acid. It should be emphasized that a different batch of oil was utilized in comparison to that of Figures 7 and 8, and there was no mound formation in the present case. The experimental conditions and the measured average current in the present experiments with brass cathode pin maintained at -12.0 kV for 43 h are listed in Table 3. The difference in the electric current between the base case (Case A) and the case with added oleic acid (Case B) most likely stems from the difference in humidity maintained, rather than the oleic acid concentration. The comparison of the deposit after cleaning the copper counter-electrode with heptane is depicted in

Figure 18. The deposit was still composed of both lighter and hair-like structures. Note that in Case B (Figure 18b) the majority of the area shown is covered with the deposit with the background seen only at the corners. The deposit in Case B is wider in comparison to Case A and additionally has a darker core at the center. All these distinctions are attributed to faradaic reactions which involve oleic acid.

Table 3. Experimental conditions and the measured average electric current for Case A and the case with added oleic acid (Case B).

Case A: Base case- canola oil	**Case B: Canola oil with added 50 g/L of oleic acid**
RH 16 – 26 %	RH 21 – 28 %
Average current = -0.05 μA	Average current = -0.13 μA
-12.0 kV to pin electrode for 43 h	-12.0 kV to pin electrode for 43 h

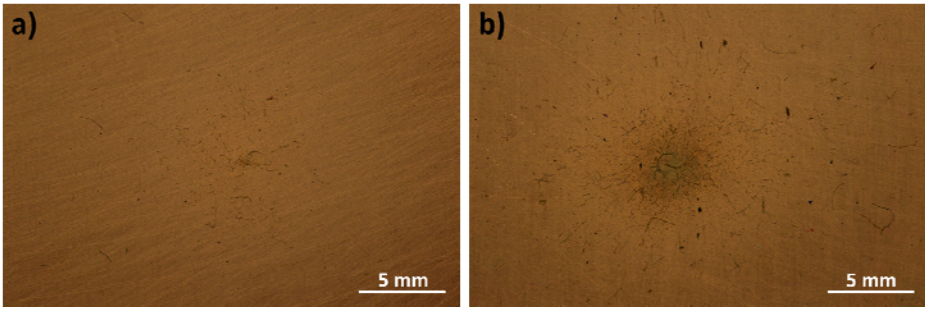

Figure 18. The image of the copper counter-electrode surface cleaned with heptane with the residual deposit accumulated in the experiment in 43 h. (a) Base case canola oil, and (b) canola oil with added 50 g/L of oleic acid.

Effect of humidity on the electric conductivity and faradaic reactions. Using the setup of Figure 6, experiments were conducted to reveal the effect of humidity on the electrical conductivity of oil. Humidity and absorbed water content are known to affect oil properties [14]. The oil was stored in a humidity-controlled chamber maintained at 33±3 % RH (relative humidity). In addition, the 47- 49 % RH case was studied under the environmental humidity conditions, to which the oil was subjected for 3 to 4 days. Also, for the experiments with 99% RH, the setup of Figure 6 was left in the humidity-controlled chamber for more than 72 h before the electrical conductivity was measured. The humidity level immediately under the free surface of oil C_{eq} in equilibrium is determined by Henry's law. Assuming the diffusion coefficient D ~ 10^{-9} m^2/s, and the characteristic depth of 1 cm, the characteristic time for 90% saturation at that depth estimated from the one-dimensional diffusion problem for water molecules in oil would be ~100 h. Therefore, in all the case presented here there should be a considerable concentration of the dissolved water in oil, albeit oil may not be fully saturated with dissolved water.

The conductivity of oil was measured for the relative humidity (RH) values: 31-35 %, 47-49 % and 99 %. The results for these cases are shown in Figure 19.

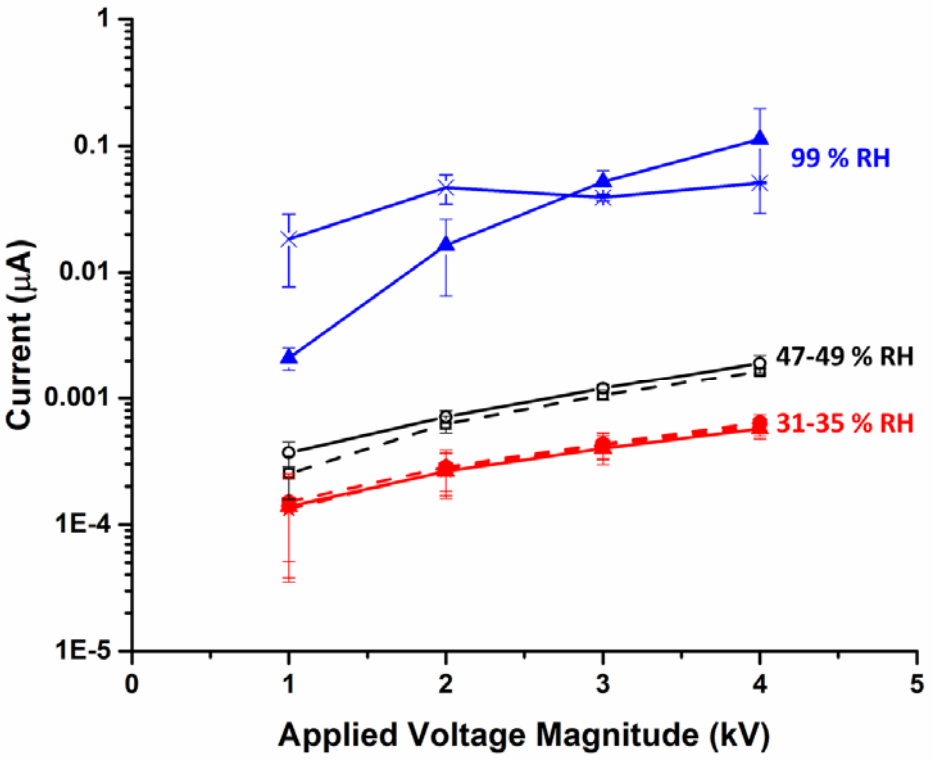

Figure 19. Electric current measured at different levels of relative humidity (RH).

Figure 19 reveals that humidity plays a significant role in the electrical conductivity of oil resulting in a nearly two orders of magnitude increase in the electric current from 31-35 % RH to 99 % RH. The 47-49 % RH case also revealed a considerable difference in the measured electric current in comparison to the 31-35 % RH case. This finding is corroborated by the results for vegetable oil published elsewhere [13]. The contribution of dissolved water can be manifold. Vegetable oil can undergo hydrolysis in presence of water to form fatty acids and alcohols. This would facilitate the electrode faradaic reactions forming metal soaps. Furthermore, water

molecules can dissociate to form proton (H^+) and hydroxyl (OH^-) ions. The protons can be directly involved in the cathodic reactions according to Eqs. (1) and (4), while the hydroxyl ions can be directly involved in the anodic reactions. In particular, hydroxyl ions can facilitate formation of the basic copper carbonates discussed in one of the previous sections. Still, the results show that the rate of faradaic reaction at the electrode is significantly enhanced in the presence of dissolved water.

Faradaic reactions in the framework of the Frumkin-Volmer-Butler model. The faradaic reactions we are dealing with belong to the following Redox type

$$Ox + nF = Red \tag{11}$$

where Red and Ox denote the cations and anions, respectively, n is an integer and F is the Faraday constant. The Frumkin-Volmer-Butler model yields the following current-voltage relation in such cases [22-23]

$$J_e = AnF\exp\left[\frac{(\alpha n - z_1)F\psi_1}{RT}\right]\left\{k_r C_{Ox}\exp\left[-\frac{\alpha nF\eta}{RT}\right] - k_s C_{Red}\exp\left[\frac{(1-\alpha)nF\eta}{RT}\right]\right\} \tag{12}$$

with A being the electrode area [in the present setup given by Eq. (10)], k_r and k_s being the pre-exponentials of the forward and backward processes (in cm/s), respectively, α being the dimensionless charge transfer coefficient, R being the universal gas constant, η being the over-potential, T being temperature, C_{Ox} and C_{Red} the concentrations of the cations and anions (in mol/cm^3), respectively, n being the number of electrons transferred, z_1 being the charge of cations (Ox) in Eq. (11), and ψ_1 being the potential close to that of the outer Helmholtz surface.

In the cathodic reduction process the second term in Eq. (12) is negligibly small and it reduces to the following equation [22]

$$J_e = Aj_0 \exp\left[\frac{(\alpha n - z_1)F\psi_1}{RT}\right]\exp\left[-\frac{\alpha nF\eta}{RT}\right] \tag{13}$$

where j_0 is the exchange current density.

For the cathodic hydrogen reduction process [the process of interest here, cf. Eq. (2), as well as for the water-related reactions associated with the effect of humidity] where according to Frumkin [22] $\alpha=1/2$ and $z_1=1$, Eq. (13) can be rearranged to the following Tafel form

$$\eta + \psi_1 = a_c + b_c \log j_e \tag{14}$$

where the electric current density $j_e=J_e/A$, and accounting for the fact that $\alpha=1/2$, $n=1$ and $z_1=1$,

$$a_c = \frac{2RT}{F}2.3\log j_0, \quad b_c = -2.3\frac{2RT}{F} \tag{15}$$

Note that the factor 2.3 arises due to conversion of natural to decimal logarithm. It should be emphasized that even though Frumkin [22] established the parameter values using water as the working fluid, a similar Eq. (2) enters the electrochemical kinetic of oils, which makes the value of $\alpha=1/2$ applicable.

Formatted: Highlight

Formatted: Highlight

On the other hand, in the anodic oxidation process on the same electrode the first term in Eq. (12) is negligibly small, and the electric current density magnitude $|j_e|$ takes the following Tafel form

$$\eta - \psi_1 = a_a + b_a \log|j_e| \tag{16}$$

where, accounting for the fact that $\alpha=1/2$, $n=1$ and $z_1=1$,

$$a_a = -\frac{2RT}{F}2.3\log|j_0|, \quad b_a = 2.3\frac{2RT}{F} \tag{17}$$

It should be emphasized that η is the difference of two potentials (a reduction potential and the potential outside the near-electrode polarized layer), which automatically accounts for the fact that potentials can be defined up to an additive constant. When the Frumkin-Butler-Volmer law

is simultaneously applied to cathode and anode in the two-electrode system of interest here, it should be guaranteed that the magnitudes of the cathode and anode currents are the same. This is achieved by assigning the antisymmetric over-potential values, namely, $(-\eta-\psi_1)\big|_{\text{cathode}} = (\eta-\psi_1)\big|_{\text{anode}}$, which is corroborated by Eqs. (14) and (16). ~~This is achieved by assigning the antisymmetric over-potential values, namely, $\eta=-V_0/2$ on the cathode and $\eta=V_0/2$ on the anode.~~ Then, Eqs. (14)-(17), indeed, reveal the same magnitudes of the cathodic and anodic currents. Note also, that this is guaranteed by the fact that $\alpha=1/2$. Not accounting for the effect of the polarized layer on the rate of faradaic reactions, i.e. not accounting for the Frumkin factor in Eq. (12), dramatically affects the values of the Tafel coefficients, skews the value of α to almost zero [9], which is intolerable for the electric current conservation in two-electrode systems.

It should be emphasized that in the setup in Figure 6 the electrodes are not plane symmetric surfaces, as the above consideration implies, but rather quite asymmetric. Still, the very top of the sharp electrode tip is parallel to the counter-electrode in a plausible agreement with the geometrical assumption made, and these are the surface areas where the most important electrohydrodynamic phenomena are anticipated. Therefore, it is essentially implied that the Frumkin-Butler-Volmer law is applied over a strictly localized domain, where the main electrohydrodynamical phenomena occur.

Equations (14)-(17) yield the following equation for the magnitude of the electric current density

$$j_e = j_0 10^{\left[(-V_0/2+\psi_1)/b_c\right]} = 10^{\left\{\left[-V_0/2-(a_c-\psi_1)\right]/b_c\right\}} \qquad (18)$$

It should be emphasized that Eqs. (11)-(18) imply the entire electrode being equipotential. This is definitely a simplified view of the electrode depicted in Figure 6c, where the electrode surface

Formatted: Highlight
Formatted: Highlight
Formatted: Highlight
Formatted: Highlight
Formatted: Indent: First line: 0.38"
Formatted: Highlight
Formatted: Indent: First line: 0"

far from the tip is covered by an insulation silicone layer. Also, this approximation does not account for the presence of the oxide islands, alloys and impurities on real electrodes. However, the approximation of Eqs. (11) - (18) is still plausible, especially over a small area near the electrode tip, where the main electrohydrodynamical phenomena occur. This means that these equations are sufficiently accurate when they are used over a strictly localized domain.

Faradaic reactions at high voltage. In the experiments, the charge carriers can dissociate in the bulk and the resulting ions discharge at the opposite electrodes as described in Eqs. (2) and (3). On the other hand, neutral species can also accept electrons at the metal-liquid interface [10], and thus become charge carriers due to such a mechanism of faradaic reactions. Namely, charge carriers can be formed or reduced at the electrode-liquid interface [10] at high voltage [12] (sometimes this is termed as ion injection, whereas in reality an electron should be transferred either to an electro-neutral compound or a molecule in a faradaic reaction). For example, $RCOO^-$ can be formed at the cathode according to the following reaction

$$2RCOO^-H^+ + 2e^- \rightarrow 2RCOO^- + H_2 \qquad (19)$$

Even in this case, the anodic process would remain similar to Eq. (3).

At higher voltage values, toroidal flows always directed away from the pin electrode were observed irrespective of the pin polarity. Such flows are illustrated in Figures 20a and 20b corresponding to -5 kV and +5 kV, respectively. Weak flows near the tip were also observed at ±1 to ±4 kV, being enhanced as the applied voltage increased. However, only above ±4 kV, the bulk flows were significant. It should be emphasized that the direction of flow remained the same irrespective of positive or negative voltage being applied to the pin (cf. Figures 20a and 20b). This can be interpreted by the above-mentioned mechanism of the corresponding faradaic reactions: neutral species losing an electron in contact with the anode (a positive pin), or neutral

species accepting an electron in contact with the cathode [a negative pin; cf. Eq. (19)]. In both cases the bulk charge has the same polarity as the pin, and accordingly the charged liquid is repelled by the Coulomb force from the pin irrespective of its polarity. This effect also influences the Tafel plot, which reveals changes in the slope at the intermediate voltage values (cf. Figure 21 discussed below).

It should be emphasized that the existing numerical models of the electrohydrodynamic flows arising due to metal electrodes sustaining electric current through a fluid (e.g. in Refs. 44 and 45) imply a given charge injection rate, whereas in reality the injected charge and the charge injection rate are not given. The present experimental results, in principle, allow one to close such a gap in the existing models and develop models accounting for the effect of faradaic reactions.

Formatted: Highlight

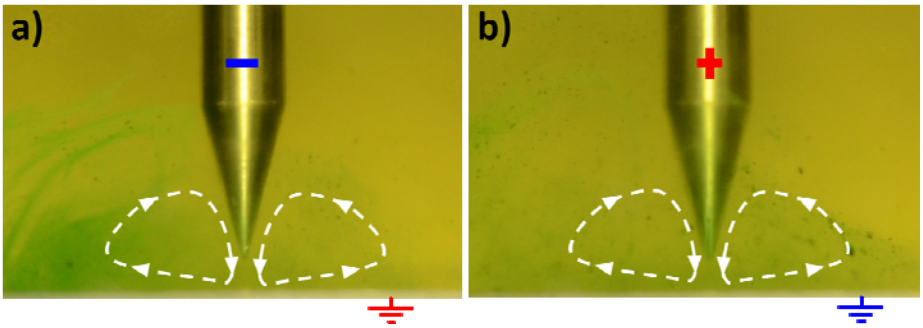

Figure 20. Toroidal vortical flows in bath of canola oil with pin electrode held at the following applied voltages: (a) -5 kV, and (b) +5 kV. Food dye is added to visualize the motion.

Note that it is also of interest to understand the effect of high voltage on vegetable oils used in electrostatic atomizers for various applications in the food processing industry. The economic advantages and sensory quality of food when electrostatic atomization was used for different

food preparation processes have been explored [44-46]. However, a matter of concern is that no consideration of the chemical changes in oil during electrostatic atomization is mentioned. At high voltages applied, the electrical stresses might facilitate formation of fatty acids as discussed above. A confirmation of the role of these different species and the accompanying faradaic reactions discussed above are important for the evaluation of suitability of the atomization technology in the food industry. Furthermore, the present results facilitate our understanding of charging of leaky dielectric liquids in electrostatic atomizers and the ways of its optimization.

Formatted: Highlight

Tafel plot. The current-voltage characteristics measured with positive and negative applied voltages at the stainless steel pin (uninsulated) and the stainless steel counter-electrode are shown in Figure 21 in the form of the Tafel plot. Uninsulated pin was utilized because the current obtained from the insulated pin was not repeatable at voltages higher than 6 kV. Figure 21 is plotted in the $\pm$ 12 kV range (i.e. for $V_0/2 = \pm 6$ kV). With α=1/2 and a specific RH value the slopes of the cathodic [Eq. (14)] and the anodic [Eq. (16)] branches are used to find the values of $a_c - \psi_1$ or $a_a + \psi_1$ for each applied voltage (since these values are supposed to be voltage-dependent [22]). The results are shown in Figure 22. The cathodic and anodic branches are close to be anti-symmetric, as expected.

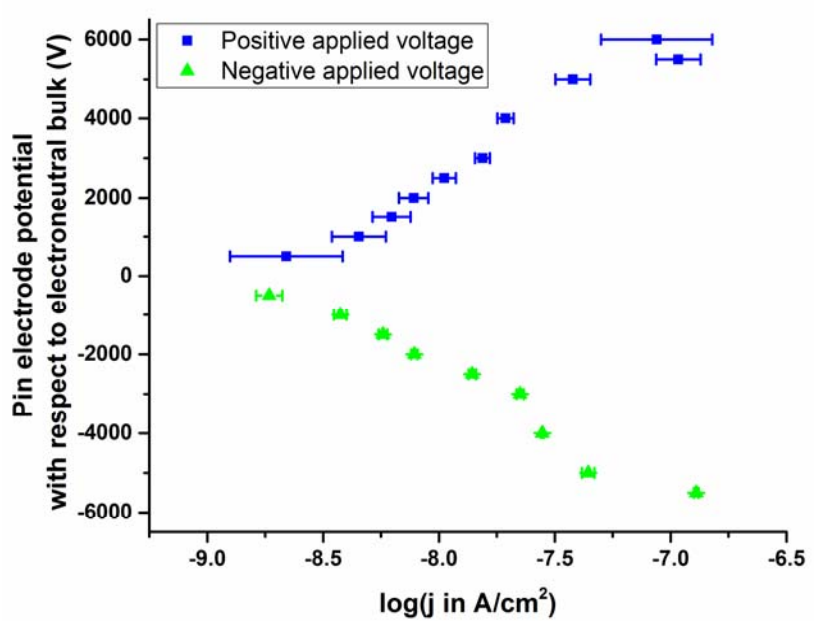

Figure 21. Current-voltage characteristics measured with positive and negative applied voltage to the pin electrode at 31-35 % RH. The pin electrode and the counter-electrode plate were made of stainless steel. The applied potential difference was in the 1-12 kV range. The inter-electrode gap was 1.8 mm.

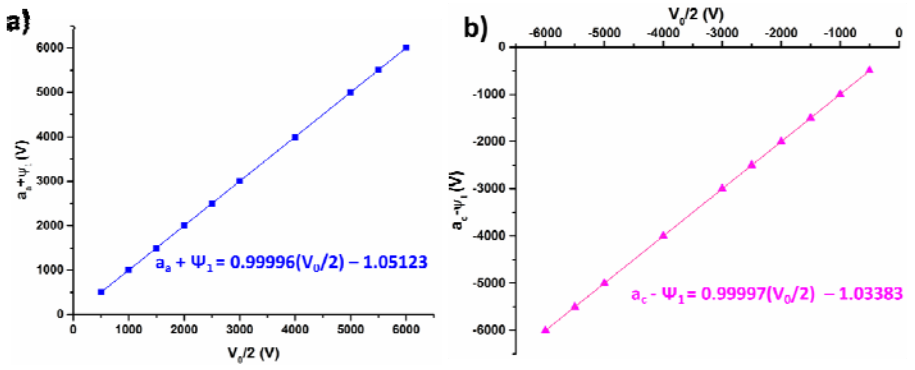

Figure 22. (a) The measured values of $a_a + \psi_1$ and (b) $a_c - \psi_1$ as a function of $V_0/2$ obtained from the corresponding anodic and cathodic branches in Figure 20.

CONCLUSION

Here we explored detailed kinetic mechanisms of the electrode faradaic reactions in vegetable oil subjected to relatively low and high voltages and carrying the electric current. Metal salts of fatty acids are the most likely products formed at the anode as the result of the anodic reactions. Also, the products of the anodic reactions revealed formation of oxides and carbonates. The latter are formed in part due to the presence of fatty acids, and in addition due to the presence of dissolved and dissociated water molecules. The cathodic reactions were associated with hydrogen reduction, with fatty acids and dissociated water molecules being the source of protons. The results revealed a very significant effect of humidity on the electrical conductivity of oil. Dry surrounding air can significantly diminish the electrical conductivity of oil. At high voltage values (with the magnitudes above 4 kV) an additional mechanism of faradaic reactions becomes significant. Namely, neutral species accept electron on the pin cathode, or lose electron at the pin anode. As a result, at any polarity a repulsive Coulomb force

emerges and acts on the fluid bulk near the pin electrode, and a vortical flow arises directed outward from the pin. It should be emphasized that in the context of the electrostatic atomization of oil, fluid layers near the electrodes polarized due to faradaic reactions are swept in the spray.

ACKNOWLEDGEMENT

This work was supported by National Science Foundation (NSF) GOALI Grant CBET-1505276. The authors wish to thank Dr. Neal Mankad and Dr. Chia-Wei Hsu for the insights and assistance with the infrared spectroscopy experiments. The authors are also grateful to Dr. Egemen Ergene for the bubble visualization and acknowledge Spraying Systems and Anthony Perri for the results from the commercial conductivity meter used for comparison with the present setup.

DECLARATION OF INTEREST: None.

REFERENCES

[1] Taylor, G. I. Electrically driven jets. Proc. R. Soc. London, Ser. A. **1969,** 313, 453-475.

[2] Melcher, J. R. Electrohydrodynamics. In Thirteens International Congress on Theoretical and Applied Mechanics; Becker, E., Mikhailov, G. K. Eds.; Springer: New York, **1973**, pp 240–263.

[3] Melcher, J. R.; Taylor, G. I. Electrohydrodynamics: a review of the role of interfacial shear stresses. Annu. Rev. Fluid Mech. **1969,** 1, 111-146.

[4] Saville, D. A. Electrohydrodynamics: The taylor-melcher leaky dielectric model. Annu. Rev. Fluid Mech. **1997,** 29, 27-64.

[5] Chang, H-C.; Yeo, L. Y. *Electrokinetically Driven Micro Fluidics and Nano Fluidics*. Cambridge University Press, New York, **2010**.

[6] Zussman, E.; Theron, S. A. Electric and magnetic parameters in liquid and gases. In Handbook of Experimental Fluid Mechanics; In *Handbook of Experimental Fluid Mechanics*; Tropea, C., Yarin, A. L., Foss, J. (Eds.); Springer, Heidelberg, **2007**.

[7] Theron, S. A.; Zussman, E.; Yarin, A. L. Experimental investigation of the governing parameters in the electrospinning of polymer solutions. Polymer **2004,** 45, 2017-2030.

[8] Shrimpton, J. S. Charge Injection Systems – Physical Principles, Experimental and Theoretical Work. Springer, Berlin, **2009**.

[9] Sankaran, A.; Staszel, C.; Sahu, R. P.; Yarin, A. L.; Mashayek, F. Evidence of Faradaic reactions in electrostatic atomizers. Langmuir. **2017,** 33, 1375-1384.

[10] Alj, A.; Denat, A.; Gosse, J. P.; Gosse, B.; Nakamura, I. Creation of charge carriers in nonpolar liquids. IEEE Trans. Electr. Insul. **1985,** 2, 221-231.

[11] Castellanos, A.; Perez, A. T. Electrohydrodynamic systems. In *Handbook of Experimental Fluid Mechanics*; Tropea, C., Yarin, A. L., Foss, J. (Eds.); Springer: Heidelberg, **2007**, pp 1317–1331.

[12] Castellanos, A. Electrohydrodynamics. Springer: New York, **1998**.

[13] Itahashi, S., Mitsui, H., Sato, T., Sone, M. State of water in hydrocarbon liquids and its effect on conductivity. IEEE transactions on dielectrics and electrical insulation, **1995**, 2, 1117-1122.

[14] Kurashige, J., Takaoka, K., Takasago, M., Taru, Y., & Kobayashi, K. State of dissolved water in triglycerides as determined by Fourier transform infrared and near infrared spectroscopy. Journal of Japan Oil Chemists' Society, **1991**, 40, 549-553.

[15] Idem, R. O.; Katikaneni, S. P.; Bakshi, N. Thermal cracking of canola oil: reaction products in the presence and absence of steam. Energy Fuels. **1996,** 10, 1150-1162.

[16] Codex standard for named vegetables oils, *Codex Stan.* 210-1999 edn.

[17] Kuppithayanant, N.; Hosap, P. Chinnawong, N. The effect of heating on vitamin E decomposition in edible palm oil. IJERD. **2014,** 5, 121-125.

[18] Tyagi, V. K.; Vasishtha, A. K. Changes in the characteristics and composition of oils during deep-fat frying. J. Am. Oil Chem. Soc. **1996,** 73, 499-506.

[19] Crossley, A.; Heyes, T. D.; Hudson, B. J. F. The effect of heat on pure triglycerides. J. Am. Oil Chem. Soc. **1962,** 39, 9-14.

[20] Zhang, Y.; Yarin, A. L. Electric current and irreversible Faradaic reaction on electrode in contact with electrolyte. J. Electrochem. Soc. **2012,** 159, 787-791.

[21] Cherepanov, G. P. *Mechanics of Brittle Fracture*. McGraw-Hill, New York, **1979**.

[22] Antropov, L. I. *Theoretical Electrochemistry*. Honolulu University Press of the Pacific, Honolulu **2001**.

[23] Bard, A. J.; Faulkner, L. R. *Electrochemical Methods Fundamentals and Applications*. John Wiley & Sons, New York, **2001**.

[24] Miller, F. Carboxylic acids as metal extractants. Talanta **1974**, 21, 685-703.

[25] van den Berg, K.J.; Burnstock, A.; de Keijzer, M.; Krueger, J.; Learner, T.; de Tagle, A.; Heydenreich, G. (Eds.) *Issues in Contemporary Oil Paint.* Springer, New York, **2014.**

[26] Wilson, G. J.; Lin, C. Y.; Webster, R. D. Significant differences in the electrochemical behavior of the α- , β- , γ- and δ- tocopherols (vitamin E). J. Phys. Chem. B **2006,** 110, 11540-11548.

[27] Brewer, M. S. Natural antioxidants: sources, compounds, mechanisms of action and potential applications. Compr. Rev. Food Sci. Food Saf. **2011,** 10, 221-247.

[28] Gulcin, A. K. T. Antioxidant and radical scavenging properties of curcumin. Chem.-Biol. Interact. **2008,** 174, 27-37.

[29] Smythe, W. R. *Static and Dynamic Electricity*. McGraw-Hill, New York, **1989**.

[30] Yarin, A. L.; Koombhongse, S.; Reneker, D. H. Taylor cone and jetting from liquid droplets in electrospinning of nano fibers. J. Appl. Phys. **2001**, 90, 4836-4846.

[31] Yarin, A. L.; Pourdeyhimi, B.; Ramakrishna, S. *Fundamentals and Applications of Micro and Nanofibers*. Cambridge University Press, Cambridge, **2014**.

[32] Guderjan, M.; Elez-Martínez, P.; Knorr, D. Application of pulsed electric fields at oil yield and content of functional food ingredients at the production of rapeseed oil. Innovative Food Science & Emerging Technologies, **2007**, 8, 55-62.

[33] Daniel, J.; Rajasekharan, R. Organogelation of plant oils and hydrocarbons by long-chain saturated FA, fatty alcohols, wax esters, and dicarboxylic acids. Journal of the American Oil Chemists' Society, **2003**, 80, 417-421.

[34] Koenig, A. E. On the stearates and palmitates of the heavy metals with remarks concerning instantaneous precipitations in insulating solutions. Journal of the American Chemical Society, **1914**, 36, 951-961.

[35] Robinet, L.; Corbeil, M. C. The characterization of metal soaps. Studies in Conservation, **2003**, 48, 23-40.

[36] Otero, V.; Sanches, D.; Montagner, C.; Vilarigues, M.; Carlyle, L.; Lopes, J. A.; Melo, M. J. Characterisation of metal carboxylates by Raman and infrared spectroscopy in works of art. Journal of Raman Spectroscopy, **2014**, 45, 1197-1206.

[37] Deng, Y.; Handoko, A. D.; Du, Y.; Xi, S.; Yeo, B. S. In situ Raman spectroscopy of copper and copper oxide surfaces during electrochemical oxygen evolution reaction: Identification of CuIII oxides as catalytically active species. ACS Catalysis, **2016**, 6, 2473-2481.

[38] Frost, R. L.; Martens, W. N.; Rintoul, L.; Mahmutagic, E.; Kloprogge, J. T. Raman spectroscopic study of azurite and malachite at 298 and 77 K. Journal of Raman Spectroscopy, **2002**, 33, 252-259.

[39] Fazal, M. A.; Haseeb, A. S. M. A.; Masjuki, H. H. Corrosion mechanism of copper in palm biodiesel. Corrosion Science, **2013**, 67, 50-59.

[40] Ergene, E. L. Investigation of the Electrostatic Atomization Method for Remote Injection and High Pressure. Doctoral Dissertation, University of Illinois at Chicago, **2012**

[41] Haidara, M.; Atten, P. Role of EHD motion in the electrical conduction of liquids in a blade-plane geometry. IEEE Trans. Ind. Appl. **1985**, IA-21, 709-714.

[42] Atten, P.; Malraison, B.; Zahn, M. Electrohydrodynamic plumes in point-plane geometry. IEEE Trans. Dielectr. Electr. Insul. **1997**, 4, 710-718.

[43] Corach, J.; Sorichetti, P. A.; Romano, S. D. Electrical properties of vegetable oils between 20 Hz and 2 MHz. Int. J. Hydrogen Energy **2014**, 39, 8754-8758.

~~[44] Barringer, S. A.; Sumonsiri, N. Electrostatic coating technologies for food processing. Annu. Rev. Food Sci. Technol. **2015**, 6, 157-169.~~[44] Perez, A. T.; Traore, P.; Koulova-Nenova, D.; Romat, H. Numerical study of an electrohydrodynamic plume between a blade injector and a flat plate. IEEE Transactions on Dielectrics and Electrical Insulation, **2009**, 16, 448-455.

[45] Traoré, P.; Daaboul, M.; Louste, C. Numerical simulation and PIV experimental analysis of electrohydrodynamic plumes induced by a blade electrode. Journal of Physics D: Applied Physics, **2010**, 43, 225502.

Formatted: Highlight

[46] Barringer, S. A.; Sumonsiri, N. Electrostatic coating technologies for food processing. Annu. Rev. Food Sci. Technol. **2015**, 6, 157-169.